International Journal of Heavy Vehicle Systems

ISSN online: 1741-5152 - ISSN print: 1744-232X
https://www.inderscience.com/ijhvs

Influence on polygon effect with characteristic parameters of guide arc branch of the crawler robot

Xiaobing Chen, Hong Zhang, Yang Liu, Jingyu Wang, Jiaqi Song

DOI: 10.1504/IJHVS.2023.10058631

Article History:

Received:	09 March 2023
Last revised:	10 March 2023
Accepted:	13 March 2023
Published online:	24 January 2024

Influence on polygon effect with characteristic parameters of guide arc branch of the crawler robot

Xiaobing Chen, Hong Zhang*, Yang Liu, Jingyu Wang and Jiaqi Song

School of Mechanical Engineering,
Taiyuan University of Science and Technology,
66 Waliu Road, Taiyuan, 030024, Shanxi, China
Email: 1810349837@qq.com
Email: hexie007@163.com
Email: 17865566339@163.com
Email: w925498255@163.com
Email: 1340458994@qq.com
*Corresponding author

Abstract: Aiming at the problem of polygon effect vibration caused by unreasonable matching between track plate and chain link pitch of crawler robot in coal mine, a method is proposed to improve polygon effect by adjusting characteristic parameters of guide arc branch. First, the theory of polygon effect and vibration of chain link is analysed. Second, the virtual simulation experiments and discussion of the crawler robot with different guide arc branch parameters are carried out by RecurDyn. Finally, the external test is carried out. The results show that with the increase of D_c and L_c, the contact forces between the observed track plate and the idler, and between the mountain damping pad and the road significantly decrease, the vibration displacement of vehicle body correspondingly decreases, and the vibration impact of the crawler robot is weakened, which provides theoretical reference for improving ride comfort of the crawler robot in coal mine.

Keywords: polygon effect; guide arc-branch; dynamics simulation; crawler robot; external test.

Reference to this paper should be made as follows: Chen, X., Zhang, H., Liu, Y., Wang, J. and Song, J. (2024) 'Influence on polygon effect with characteristic parameters of guide arc branch of the crawler robot', *Int. J. Heavy Vehicle Systems*, Vol. 31, No. 1, pp.32–48.

Biographical notes: Xiaobing Chen received his BS in Vehicle Engineering from the School of Mechanical Engineering, Henan University of Technology, Zhengzhou, China, in 2019. Now he is a MS student in Mechanical Engineering at Taiyuan University of Science and Technology, Taiyuan, China. His research interests cover mechanical dynamics and vibration monitoring.

Hong Zhang received his PhD in Mechanical Engineering from Taiyuan University of Technology in 2008. Now he is a Professor at Taiyuan University of Science and Technology, Taiyuan, China. His research interests include machinery and special vehicle dynamics, coal mining equipment development, fluid transmission and control, dynamic monitoring, and fault diagnosis.

Yang Liu is currently a Master's degree candidate in Mechanical Engineering at Taiyuan University of Science and Technology, Taiyuan, China. His research interests covers dynamic testing and wireless sensing systems.

Jingyu Wang is a Master student majoring in Mechanical Engineering at Taiyuan University of Science and Technology, China. His research interests include degradation assessment and life prediction.

Jiaqi Song is currently a Master's degree candidate in Mechanical Engineering at Taiyuan University of Science and Technology, Taiyuan, China. His research interests cover CAE analysis of the contact between crawler robot and complex pavement.

1 Introduction

Crawler robot in coal mine is a kind of special robot, which is widely used in complex and harsh working environments such as underground roadway excavation, roadway inspection, emergency rescue and so on. Due to the crawler robot's long-term operation in water, unstructured terrain and closed and restricted environment (Yang et al., 2020), sometimes the matching of the track shoe pitch and link pitch is not reasonable, and vibration of the crawler chain ring meshing with the driving wheel results in the polygonal movement and non-uniformity of the crawler chain ring when the robot is working, which has a great impact on the operational stability of the crawler robot in coal mine (Ramamurthy et al., 2018).

In terms of polygon effect of chain drive and vibration test, Liu et al. (2021) analysed polygon effect of chain drive by ADAMS and concluded that with the wear of sprocket, the instability and impact load of chain system drive increased significantly. Chen et al. (2019) established a vehicle-track-subgrade model, and measured that the short-wave excitation generated by wheel polygon induced high-frequency wheel-rail interaction and enhanced wheel-rail vibration. Wang et al. (2020) studied the influence of wheel polygon on the dynamic response of the transmission system and concluded that the high frequency fluctuation of gear meshing force was caused by wheel polygon wear. Meng et al. (2011) established mathematical models of different stages in the meshing process of the internal meshing toothed chain, and obtained the meshing track of the internal meshing toothed chain by fitting the least squares method. Tao et al. (2017) used RecurDyn software to simulate and analyse the polygon effect and meshing impact of chain drive. Yang et al. (2017) established a real-time motion state mathematical model of the driven sprocket, solved the equation through the fourth-order R-K method, and concluded that the chain drive is actually a process of 'creeping forward'. Liao et al. (2022) studied the influence of wheel polygon wear on the stability and safety of train operation, and concluded that the influence of high-order wheel polygon wear on axle box system is greater than that of low-order wheel wear. Tao et al. (2021) analysed the formation process of wheel polygon and found that the inherent vibration of wheel set is the core intrinsic factor of wheel polygon. Zhang et al. (2012) proposed a chainsaw polygon dynamics analysis method and compared the results with the traditional chaindrive polygon effect dynamics analysis method.

The above research provides theoretical guidance for the wear and vibration induced by polygon effect of sprocket, but the polygon effect of track chain ring needs further study. By combining basic theory, simulation and experiment, this paper explores the influence of characteristic parameters of different guiding arc branch on the reduction of track chain polygon, which provides theoretical reference for improving the ride comfort of coal mine crawler robot.

2 Characteristic parameters and polygon effect of guide arc branch

2.1 Characteristic parameters of arc branch of track link

The structure of track link includes free branch, arc branch, working branch and support branch. Arc branch is located in the idler, towing sprocket and roadwheel part of the track, the idler guides track winding, the use of tensioning device to control the movement of the idler, so as to adjust the track tension, to prevent track chain jump and chain off caused by power loss.

The characteristic parameters of the arc-shaped branch between the idler and its adjacent first roadwheel are shown in Figure 1.

Figure 1 Characteristic parameter diagram of guide arc support

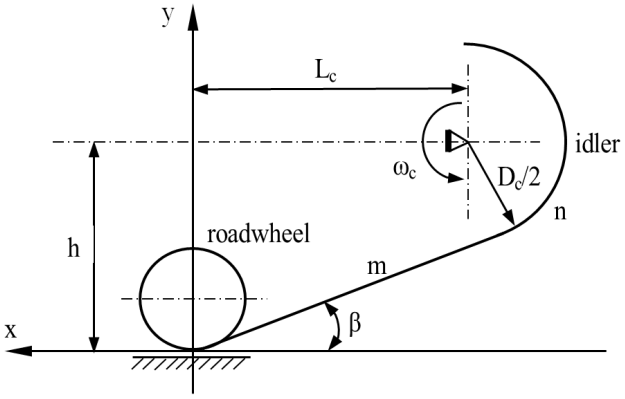

where D_c is the diameter of the idler, mm; L_c is the distance between the idler and the first adjacent roadwheel, mm; β is track approach angle; h is the height of the centre of the idler from the ground, mm; ω_c is the angular velocity of the idler, rad/min; m and n are the length of arc branch of the idler (mm).

2.2 Polygon effect and vibration

The unilateral track driving mechanism is simplified. It is assumed that there is no interference between the track plate and the adjacent connecting plate in the process of track movement, there is no stuck chain phenomenon, and the track plate keeps uniform motion. The motion velocity analysis of track link is shown in Figure 2.

Figure 2 Analysis of the movement speed of track link

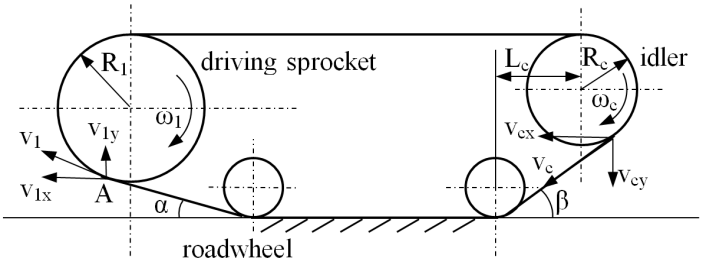

The track link pulls the track plate forward at the driving sprocket A, while other track links around the driving sprocket do not pull the track directly. Therefore, the movement speed of the track plate is completely determined by the movement of the track link at A. The linear velocity of the track link moving with the driving sprocket at place A is v_1, and the included angle between the direction and the horizontal direction of the road is. Therefore, the speed of the track link at place A for traction track movement is (Cui et al., 2018) as follow:

$$v_{1x} = v_1 \cos\alpha = R_1\omega_1 \cos\alpha \tag{1}$$

where R_1 is the dividing circle radius of the driving sprocket, mm; ω_1 is the rotation angular speed of the driving sprocket, rad/min; α is the departure angle.

The driving sprocket in the traction track to do variable speed movement at the same time, the idler, as a result of the friction of the track plate, is pushed to turn in ω_c.

Since the Angle between the direction of the track link velocity v_{cx} and the direction of the linear velocity at B is β, the linear velocity of the track link at B along the circumference is as follow:

$$v_c = R_c\omega_c = \frac{v_{cx}}{\cos\beta} \tag{2}$$

where R_c is the radius of the idler, mm; ω_c is the angular velocity of the idler, rad/min; β is the angle of approach.

From this, the angular velocity of the idler is as follows:

$$\omega_c = \frac{v_{cx}}{R_c \cos\beta} \tag{3}$$

In the transmission process, the horizontal speed of the track link at point A and point B is the same, that is, $v_{1x} = v_{cx}$, so the following relation is satisfied in the movement process of the track link:

$$\frac{\omega_1}{\omega_c} = \frac{R_c \cos\beta}{R_1 \cos\alpha} = \frac{D_c \cos\beta}{D_1 \cos\alpha} \tag{4}$$

where D_1 is the diameter of the driving sprocket, mm; D_c is the diameter of the idler, mm.

According to formula (4), when driving sprocket diameter D_1, approach angle β and departure angle α remain unchanged, idler diameter D_c increases, idler angular velocity decreases and polygon effect weakens.

It can be seen from Figure 1 that the approach angle β can be represented by the distance L_c between the idler and its adjacent first roadwheel:

$$\cos\beta = \frac{L_c}{\sqrt{L_c^{\ 2} + (h - R_c)^2}} \tag{5}$$

where L_c is the distance between the idler and the adjacent first roadwheel, mm; h is the horizontal distance between the centre of the idler and the ground, mm.

According to formula (4) and (5), D_1, D_c and ω_1 remain unchanged, L_c increases, cosβ increases, idler angular velocity ω_c decreases, polygon effect decreases significantly, and vibration and impact weaken.

Track in the process of advance, the speed of the driving sprocket and the idler are always changing, so it will cause the change of inertia force and the corresponding dynamic load. If the apparent driving sprocket rotates at a constant speed:

$$\mathrm{a}_{1y} = \frac{dv_{1x}}{dt} = \frac{d}{dt}(R_1\omega_1\cos\alpha) = -R_1\omega_1^2\sin\alpha \tag{6}$$

Namely,

$$(a_{1y})_{\max} = \mp\frac{\omega_1^2 p}{2} \tag{7}$$

The inertial forces of the guide wheel due to angular acceleration are as follows:

$$F_{cy} = \frac{J}{R_2}\frac{d\omega_{cy}}{dt} \tag{8}$$

where the moment of inertia of J driven system is converted to the idler shaft, kg·m^2; a_{1y} is the vibration acceleration in the vertical direction of the driving sprocket, m·s^{-2}; F_{cy} is the vertical vibration inertia force of the idler, N; ω_{cy} is the angular velocity of the idler, rad/s, p is the pitch of driving wheel teeth, mm.

The greater the angular velocity ω_1 of the driving sprocket, the greater the angular velocity ω_c of the corresponding idler, the more intense the inertial impact force between the idler and the track plate, and the greater the dynamic load of the track link in the vertical direction.

The polygon effect of mine track link is mainly represented by vibration acceleration value (g) and acceleration power spectral density function Ga(f) (Qiao et al., 2021). The vibration acceleration value is mainly divided into the weighted acceleration value of vertical, longitudinal and transverse vibration. This paper mainly analyses the vertical weighted acceleration g. The direct integral of the weighted acceleration self-power spectral density function Ga(f) is used to calculate a_ω:

$$a_w = \left[\int_{0.5}^{80}\omega^2(f)G_a(f)\mathrm{d}f\right]^{1/2} \tag{9}$$

where Ga(f) is power spectral density function; f is the frequency; $\omega(f)$ is the frequency weighting function.

The larger the vehicle body vibration acceleration g, the more obvious the polygon effect of track link, and the wider the range of energy concentrated in the high frequency region obtained by the power spectral density function Ga(*f*) for the same reason.

3 Dynamic simulation and analysis of crawler robot

Based on the contact force values between the observed track plate and idler, the observed mountain damping pad and the hard road, as well as change in vibration displacement of the crawler robot body, the influences of different characteristic parameters D_c and L_c on the polygon effect of the track link were analysed.

3.1 Construction of simulation model for crawler robot

The crawler robot model established by the 3D software Solidworks is shown in Figure 3, which is composed of driving sprocket, roadwheels, idler, towing sprockets, track plates, tensioning mechanism and mountain damping pads (Zhang et al., 2015, 2020). It is saved in Parasolid (* x_t.) format and imported into the dynamics software Recurdyn subsystem to set constraints, contact and other parameters.

Figure 3 Simulation model of crawler robot (see online version for colours)

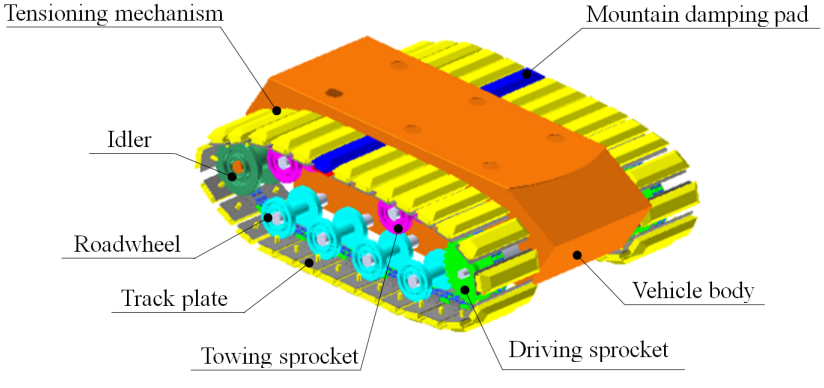

In order to accelerate the simulation speed, each axle and vehicle body are designed as a whole. The internal battery, driving motor and decelerator of the crawler robot body are replaced with an equivalent mass block. By applying a moving pair to the idler shaft to adjust the displacement of the tensioning mechanism, the track pre-tensioning force is kept between 8% and 10% of the vehicle weight before the driving sprocket starts to rotate (Meng et al., 2015), and the tensioning mechanism and the vehicle body are simplified into one.

The rigid contact between the caterpillar robot simulation model and the rigid pavement was established in RecurDyn subsystem, and Solid to Solid was added. The contact parameters mainly included the stiffness coefficient *K*, 2855 N/m; Damping coefficient *C*, 5.7 N·s/mm; Dynamic friction coefficient *mud*, 0.25; Static friction coefficient *mus*, 0.3.

The dynamic model is usually driven by If or Step function. In this paper, Step function is used to drive the crawler robot simulation model. The driving function is step (time, 0.4, 0, 0.6, 3.14) applied on the rotation pair of the driving sprocket, and the moving function of the tensioning device is step (time, 0.1, 0, 0.3, 8). Where, within 0.1 s, the crawler robot falls to the ground freely, 0.1–0.3 s is the tensioning track process of the tensioning mechanism moving idler shaft, and the driving sprocket speed is 0 rad/s during this period. Within 0.4s – 0.6s, the speed of the driving sprocket increases from 0 rad/s to 3.14 rad/s; Keep 3.14 rad/s uniform motion after 0.6 s, that is, the vehicle speed is 1.15 km/h. During the simulation process, the sampling frequency is 200 Hz and the sampling time is 20 s.

3.2 Influence of characteristic parameter D_c on polygonal effect of track link

A group of matching track plate and mountain damping pad were randomly selected from the free branch segment of the unilateral track link as the research observation object, and the idler diameter D_c was taken as 130 mm, 160 mm and 180 mm, respectively, to analyse the variation rule of the contact force between the observed track plate and idler. The crawler robot walked 3 circles in 20 s, and the contact collision between the track plate and the idler was observed for 3 times.

Figure 4 shows the variation of the observed contact force between track plate and idler with time t under different characteristic parameters D_c. As can be seen from the Figures 4, 0~1.6s ago, the observed track plate was in the free branch segment, and did not have contact with the idler, and the contact force was 0 N. From 1.6 s to 2.4 s, the observed track plate is in contact with the idler, and the contact force between the two gradually increases and then decreases. Finally, the observed track plate is out of contact with the idler, and the contact force is 0 N. When the D_c is 130 mm, the maximum contact force is 1850 1N. The maximum contact force of 160 mm and 180 mm is 534 N and 490 N, respectively. With the increase of characteristic parameter D_c, the angular velocity ω_c of idler decreases, and the polygon effect weakens. The peak contact force between the observed track plate and idler gradually decreases, and the degree of contact collision decreases, and the track motion is relatively stable. When D_c increased to more than 160 mm and continued to increase, the observed trend of contact force between track plate and idler would not change much.

Figure 5 shows the variation rule of the contact force between the observed mountain damping pad and the hard pavement with time t under different characteristic parameters D_c. As can be seen from the Figure 5, the contact force is the maximum when the mountain damping pad is just in contact with the road surface, and each contact force increases compared with the last one, which is mainly caused by the inertial impact of movement. When the motion is stable, the peak value of the contact force is 2880 N when the D_c is 130 mm. The peak value of 160 mm and 180 mm contact force decreases, and the peak value is 2450 N and 1850 N respectively. With the increase of D_c, the contact force between the observed mountain damping pad and the hard pavement gradually decreases, and the collision degree weakens. The increase of D_c is helpful to improve the life of the crawler robot moving parts. However, parameter D_c can only properly adjust the track polygon effect. When D_c reaches about 180 mm, the track link polygon effect has little decreasing trend.

Figure 4 Contact force between the observed track plate and the idler under different characteristic parameter D_c (see online version for colours)

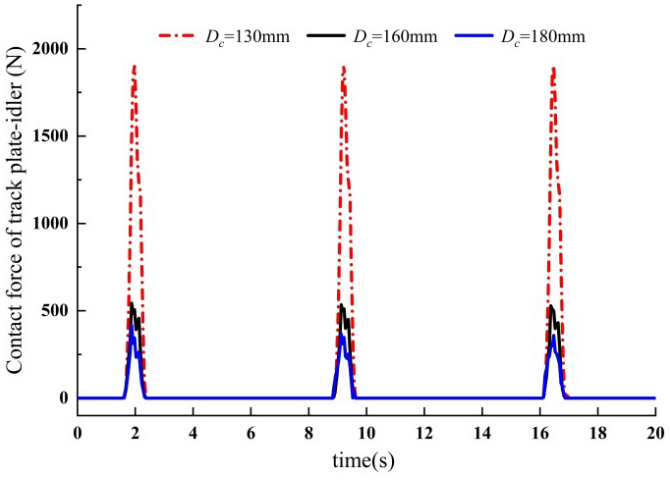

Figure 5 Contact force between the observed mountain damping pad and hard pavement under different D_c (see online version for colours)

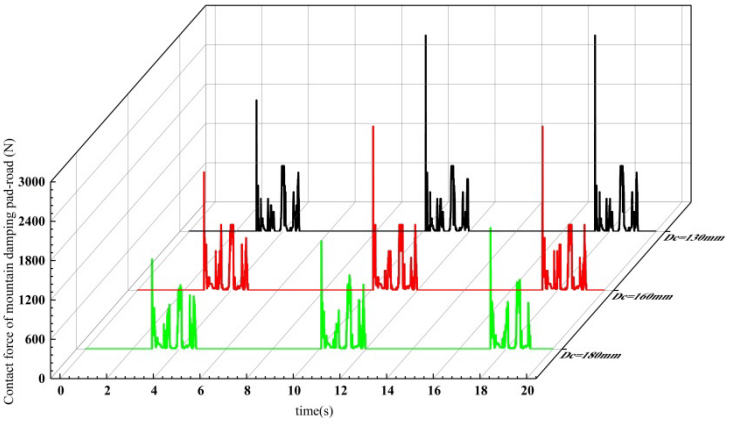

3.3 Influence of characteristic parameter L_c on polygonal effect of track link

Figure 6 shows the variation rule of the observed contact force between track plate and idler with time t under different characteristic parameters L_c. Among them, the distance L_c between the idler and the first adjacent roadwheel is 160 mm and 200 mm respectively. Two kinds of idlers with diameter of 130 mm and 160 mm were used for analysis. As can be seen from the Figure 6, when D_c is unchanged, the peak value of the contact force between the observed track plate and the idler slightly increases with the increase of L_c. When the observed track plate rotates to be tangent to the idler and perpendicular to the direction of forward motion, the maximum contact force appears. When the idler diameter is 130 mm, the L_c is 160 mm and the maximum contact force is 1922 N and 2385 N. When the idler diameter is 160 mm, the L_c is 160 mm and 200 mm, and the maximum contact force is 566N and 690N. This is because the D_c size is too

small, the approach angle β is large, appropriate increase of L_c has no obvious effect on reducing the polygon of track chain ring, so the change trend of contact force is weak.

Figure 6 Contact force between the observed track plate and the idler under different L_c (see online version for colours)

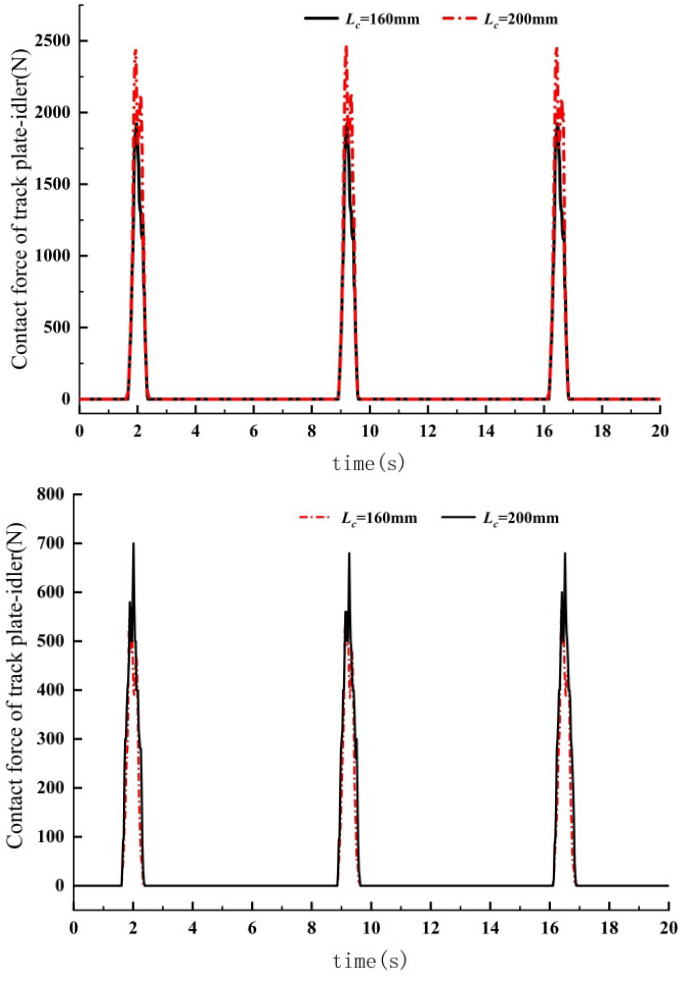

Figure 7 shows the variation of contact force between the observed mountain damping pad and hard pavement with time t under different characteristic parameters L_c As can be seen from Figure 7, D_c remains unchanged and L_c • increases, the contact force between the observed mountain damping pad and the road decreases. When the parameter L_c was increased, the arc branch of idler m was lengthened, the approach angle β between the arc branch of idler and road surface was reduced, the contact and collision degree between track and road surface was weakened, and the polygon effect of track link was reduced. When the observed mountain damping pad just contacts with the road surface, the maximum contact force appears. When the idler diameter is 130 mm, the maximum contact force is 2850 N and 1730 N when the parameter L_c is 160 mm and 180 mm. Similarly, when the idler diameter is 160 mm, the maximum contact force is 2500 N and

1800 N when the parameter L_c is 160 mm and 180 mm. The contact force between the mountain damping pad and the hard pavement increases gradually next time, which is mainly caused by the inertia impact.

3.4 Influence of D_c and L_c changes on vehicle body vibration

The influence of characteristic parameters D_c and L_c on the polygon effect of track link was analysed by analysing and comparing the vibration displacement variation in the vertical direction of vehicle centre of gravity. Figures 8 and 9 respectively show the comparison results of the vertical vibration displacement of the crawler robot in the simulation model under different characteristic parameters D_c and L_c.

Figure 7 Contact force between the observed mountain damping pad and hard pavement under different L_c (see online version for colours)

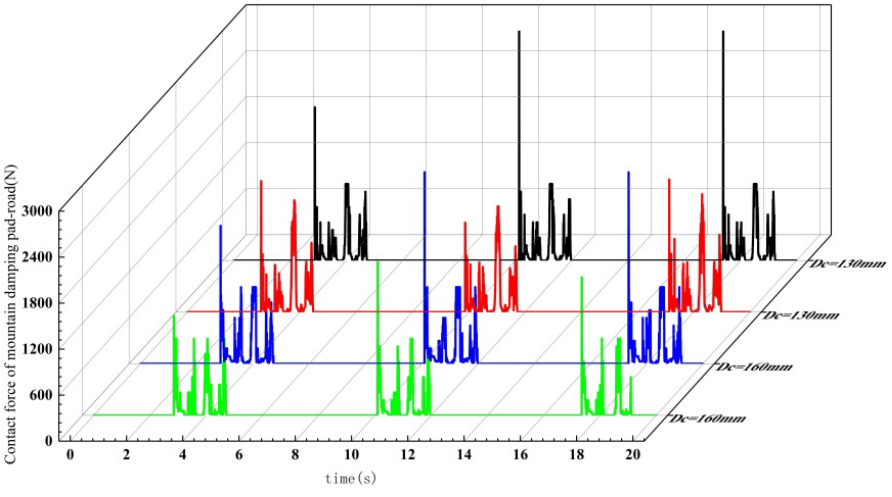

Figure 8 Vertical vibration displacement of vehicle body under different characteristic parameters D_c (see online version for colours)

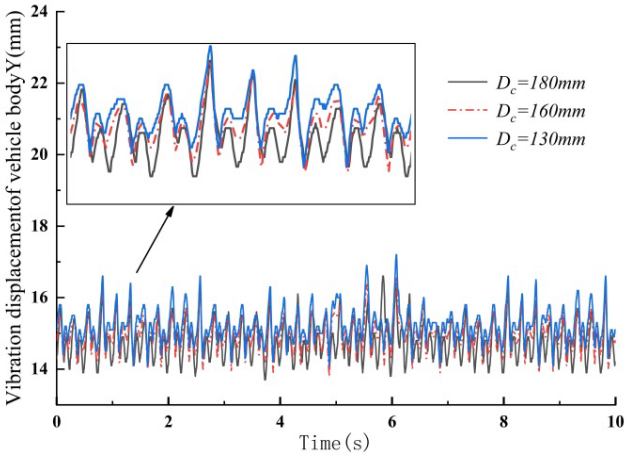

As can be seen from Figures 8 and 9, the vertical vibration displacement of vehicle body shows a downward trend with the increase of characteristic parameters L_c and D_c. The D_c values are 130 mm, 160 mm and 180 mm, and the peak values of vehicle body vibration displacement are 16.5 mm, 16.3 mm and 16.0 mm. When L_c is 160 mm and 200 mm, the peak value of vehicle body vibration displacement variation is 16.4 mm and 15.1 mm, respectively. The main reason is that the characteristic parameters L_c and D_c of the idler arc segment increase, and the impact vibration between the track and the ground in the idler arc segment is weakened, thus reducing the vibration of the vehicle, indirectly flattening the impact load brought by the polygon effect of the track link, which reduces the vibration amplitude of the crawler robot vehicle body and makes the track movement force transfer stable. The larger peak value is mainly the impact vibration will occur when each mountain damping pad starts to contact with the road surface, while the smaller peak value is generated by the driving sprocket rotation, gear meshing contact collision with the link.

Figure 9 Vertical vibration displacement of vehicle body under different characteristic parameters L_c (see online version for colours)

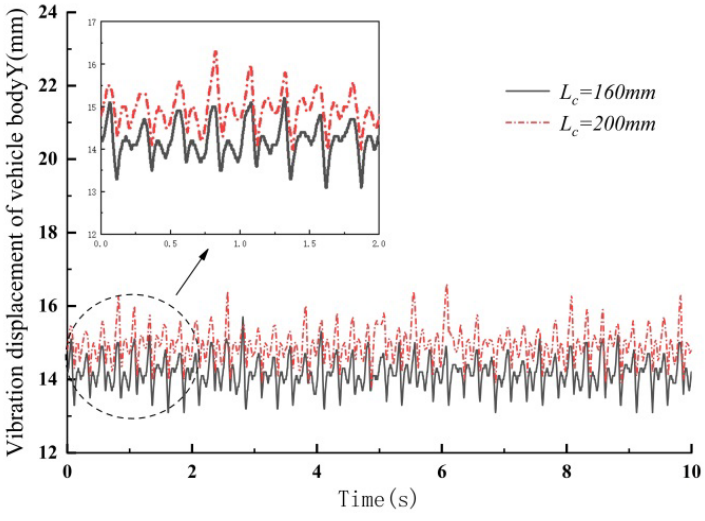

The simulation curve analysis of contact force and vibration displacement shows that the characteristic parameters of arc branch segment $D_c = 160$ mm and $L_c = 160$ mm, the vibration impact of the crawler robot is weak, the polygon effect of the crawler robot is weakened, and the movement is the most stable, so the external test analysis is carried out on it.

4 External test

The distance between the track plate and the track link is not reasonable, and the polygon effect severely affects the movement of the crawler robot, reducing the transmission stability and service life. Therefore, the vibration and impact brought by the polygon effect are analysed specifically through the external test.

The test was conducted on hard pavement on campus. Figure 10 shows the driving state test of crawler robot on hard pavement. The crawler robot has remote control driving function, built-in dynamic torque sensor and can carry small equipment. DH5902N data acquisition system of Donghua Company, vibration acceleration sensor and DYN-200 dynamic torque sensor of Bangbu Ocean Sensor Company were used as test instruments. As shown in Figure 10, acceleration sensors #1~#5 are arranged. #1 is arranged in the side position of the adjacent vehicle body of the planetary reducer, #2 is arranged in the contact area between the supporting sprocket shaft and the side of the vehicle body, #3 is arranged in the centre of gravity at the bottom of the vehicle body, and #4 and #5 are arranged in the contact area between the two roadwheel axles adjacent to the idler and the vehicle body. The DYN-200 dynamic torque sensor is positioned between the drive motor and the planetary reducer.

Figure 10 Driving state test of crawler robot on hard pavement (see online version for colours)

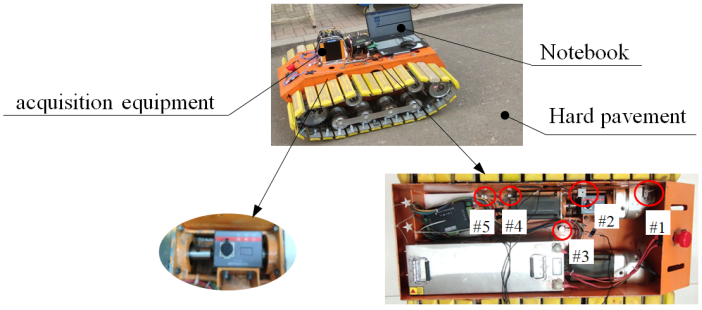

In the test, the speed data of the drive motor was collected, and the speed data was passed through the speed-time curve with the output frequency of 200 Hz at the uniform point, and the average value was taken and loaded onto the driving sprocket of the crawler robot in the simulation model to drive the simulation model to rotate. Figure 11 shows the speed – time curve of the crawler robot test on hard pavement.

Figure 11 The speed signal of vehicle (see online version for colours)

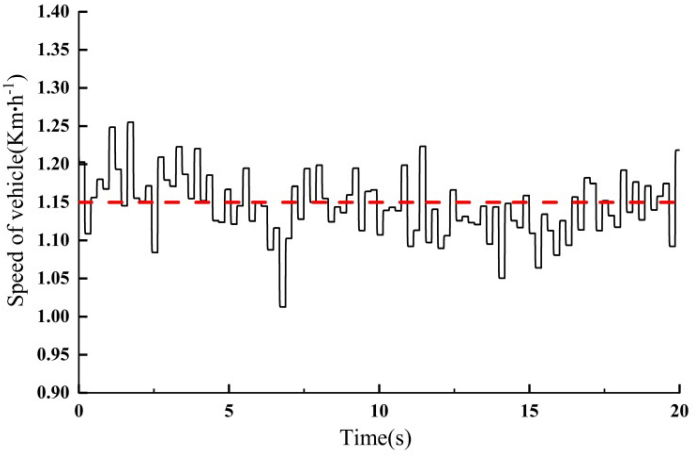

During the test, the speed was maintained at 1.15 km/h, the acquisition frequency was 2 kHz, and the time was 60 s. In order to study the influence of the characteristic parameters of the idler arc branch of the crawler robot on the polygon effect of the track link on the hard pavement, at least 3 groups of vibration data were collected in this experiment.

5 Discussion of experimental and simulation results

Fast Fourier transform (FFT) was applied to the vibration acceleration measured in the test. Figure 12 shows the vibration acceleration spectrum of vehicle body measurement points #1~#5.

Figure 12 Vibration acceleration spectrum of measuring point (see online version for colours)

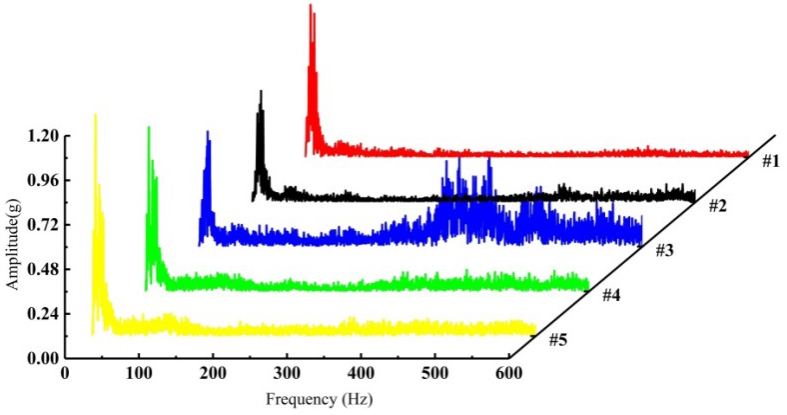

As can be seen from Figure 12, measuring points #1~#5 are the corresponding spectrum analysis of vehicle body measuring points, in which the motion process of the crawler robot is mainly low-frequency vibration, and part of it is high-frequency vibration. The main reason is that the excessive distance ratio between the track plate and the chain link leads to the intense polygon effect, resulting in the intense impact vibration between the track and the hard pavement. The frequency spectrum curve shows that the low frequency part of the vibration signal of the crawler robot vehicle body is mainly the integral multiple frequency of the road roughness frequency, the driving sprocket snapping frequency and the rotation frequency.

As shown in Figure 13, in order to compare the simulation and test vibration acceleration curves of the crawler robot on the hard pavement surface, and to accurately analyse and compare the vibration signals of measuring point #3, the vibration signals collected in the test are equally taken at the simulation frequency of 200 Hz and then plotted for analysis (Zhang et al., 2022).

As can be seen from Figure 13, on the hard road surface, the crawler robot maintains a constant speed of 1.15 km/h, and most of the simulated acceleration curves of the crawler robot fluctuate within ±2.3 g, while the test acceleration curves fluctuate within ±2.0 g, with a small difference between the two. This part of vibration is mainly caused by the meshing contact between the driving sprocket and the track link and the friction

and collision between the track plate and the wheels. Among them, the peak value of the simulated acceleration spike is close to 2.5 g. The main reason is that part of the modelling process of the crawler robot is simplified, which is different from the actual moving part of the crawler robot, resulting in intensified collision between the rigid body and the rigid body. At the same time, the Angle between the idler arc branch and the road is large.

Figure 13 Comparison of vibration acceleration curves of hard pavement (see online version for colours)

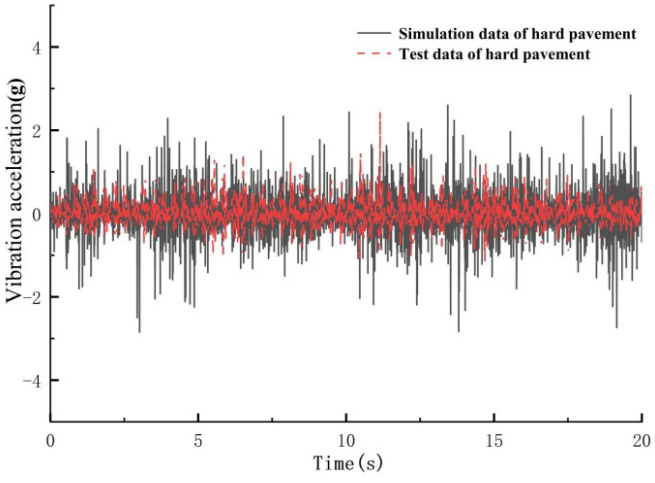

The power spectral density function is used to calculate the power spectral density curve of the crawler robot on hard pavement, as shown in Figure 14. In the power spectral density curve, the low frequency part mainly focuses on 0~30 Hz, the low frequency band 1~2 Hz mainly reflects the natural frequencies of pitch vibration and vertical vibration of the body, and the lower frequency band 4~10 Hz mainly includes the wheelbase effect caused by the wheelbase of the roadwheel and the overall vibration effect of the track link. The geometric effect of the track link can suppress the wheelbase effect in the rigid crawler robot model, but the natural vibration effect of the rigid track link is more significant.

The frequency of the periodic excitation caused by the distance between the track link and the excitation caused by the polygon effect generated by the meshing between the track link and the driving sprocket is related to the pitch and vehicle speed, where $f_t = u/3.6t_T$. In this test, when the distance between the track link is $t_T = 19.02$ mm and the average vehicle speed $u = 1.15$ km/h, the number of driving sprocket teeth is 26, then the periodic excitation frequency generated by the distance between the track link is $f_t = u/3.6t_T$, that is, $f_t = 16.8$ Hz, the driving sprocket rotation frequency f_n is 0.5 Hz, and the engagement frequency f_m between the driving sprocket and the chain link is 13 Hz. Therefore, the smaller the distance between track links and the higher the speed, the more intense the polygon effect of track link and the more obvious the vibration amplitude.

Figure 14 Power spectral density curve of vehicle body centre of gravity (see online version for colours)

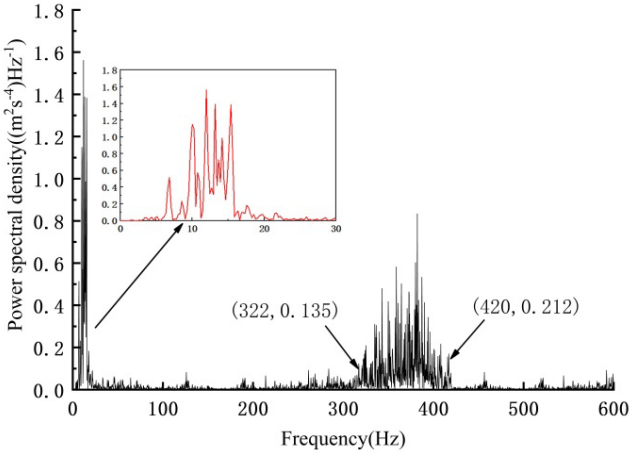

As can be seen from Figure 14, the high frequency part is above 30 Hz and concentrated between 322 Hz and 420 Hz. The frequency band of the high frequency component of the vehicle body vibration when the crawler robot is driving on the hard road is relatively wide. This is because the speed of the crawler robot presents a large disturbance in the test, which makes the vibration frequency related to the distance between the track plate and the track link constantly change. The high frequency vibration generated at the centre of gravity of the vehicle body has a wide frequency range and concentrated energy. On the one hand, it is caused by the unsteady installation of the driving motor and the vibration of the rotating parts inside the vehicle body. On the other hand, the pitch of the track plate is four times that of the track link, which is too large. As a result, the impact load between the track plate and wheels, and other contact objects during the robot driving is severe, which seriously affects the driving instability. In addition, the uneven quality of the left and right sides of the body is also one of the reasons for excessive vibration.

6 Conclusion

1 The relationship between polygon effect of track link and characteristic parameters D_c and L_c of guide arc branch was deduced. The impact vibration of idler and contact parts, and the change law of inertia force and dynamic load of crawler robot were given under the change of D_c and L_c.

2 Through simulation analysis, the observed contact force between track plate and idler, the contact force between mountain vibration cushion and hard pavement, and the variation rule of vehicle body vibration displacement with the characteristic parameters D_c and L_c of guide arc branch were analysed. It was obtained that when the parameters D_c was 160 mm and L_c was 160 mm, it was beneficial to improve the polygon effect of chain link of the crawler robot.

3 The power spectral density curve shows that the vibration frequency of vehicle body is mainly concentrated in the low frequency region of 0~30 Hz, and the high frequency vibration range is 322~420 Hz. The vibration acceleration value of vehicle body mainly fluctuates between ±2.3 g and ±2.0 g in simulation test and road test, and part of the peak value is 2.5 g. Because the approach angle β between the guide arc branch and the road is too large, the impact between the track plate and the road is severe.

Acknowledgements

The authors would like to thank the Research Project Supported by the National Natural Science Foundation of China (Grant No. 52075355). The Key R&D Projects in Shanxi Province (Grant No. 202202100401012).

References

Chen, M., Zhai, W.M. and Ge, X. (2019) 'Analysis of wheel-rail dynamic characteristics due to polygonal wheel passing through rail weld zone in high-speed railways', *Chinese Science Bulletin*, Vol. 64, No. 25, pp.2573–2582.

Cui, X.B., Zhang, H. and Shi, T. (2018) 'Ride comfort analysis of tracked vehicle based on nonuniform coefficient of link', *Chinese Journal of Engineering Design*, Vol. 25, No. 1, pp.71–78.

Liao, X.K., Yi, C. and Zhang, Y. (2022) 'A simulation investigation on the effect of wheel-polygonal wear on dynamic vibration characteristics of the axle-box system', *Engineering Failure Analysis*, Vol. 139, No, 106513, pp.1350–6307.

Liu, Y., Liu, Z.Z. and Fu, Z.M. (2021) 'Analysis of the influence of polygon effect and worn sprocket on chain system operation based on Adams simulation', *Modern Manufacturing Technology and Equipment*, Vol. 57, No. 6, pp.50–54.

Meng, F.Z., Dong, C.G. and Feng, Z.M. (2011) 'Research on meshing 'Track and polygon effect of a new silent chain with inner meshing mechanism', *China Mechanical Engineering*, Vol. 22, No. 16, pp.1891–1895.

Meng, L., Li, X.L. and Qiu, S. (2015) 'Influence analysis of tracks on body vibration for a tracked vehicle', *Vehicle and Power Technology*, Vol. 140, No. 04, pp.1–5+41.

Qiao, X.Y., Jin, Y. and Duan, Y. (2021) 'Tracked vehicle vibration response analysis based on power spectrum method in consideration of the influence of track circuit', *Journal of Vibration and Shock*, Vol. 40, No. 18, pp.94–101.

Ramamurthy, N.V., Vinayagam, B.K. and Roopchand J. (2018) 'Comfort level refinement of military tracked vehicle crew through optimal control study', *Defence Science Journal*, Vol. 68, No. 3, pp.265–272.

Tao, D.B., He, C. and Fan, X.B. (2017) 'Study on simulation of chain drive' dynamic behavior based on RecurDyn', *Journal of Mechanical Strength*, Vol. 39, No. 4, pp.986–990.

Tao, G.Q., Liu, X.L. and Wang, Z.F. (2021) 'Formation process, key influencing factors, and countermeasures of high-order polygonal wear of locomotive wheels', *Journal of Zhejiang University-Science A*(*Applied Physics and Engineering*), Vol. 22, No. 1, pp.70–85.

Wang, Z., Cheng, Y. and Mei, G. (2020) 'Torsional vibration analysis of the gear transmission system of lighspeed trans with wheel defet', *Proceedings of the Institution of Mechanical Engineers', Journal of Rail and Rapid 'Transit'*, Vol. 234, No. 2, pp.123–133.

Yang, J.J., Zhang, Q. and Wang, C. (2020) 'Status and development of robotization research on roadheader for coal mines', *Journal of China Coal Society*, Vol. 45, No. 8, pp.2995–3005.

Yang, R.M., Zhang, X.C. and Han, J.X. (2017) 'Mathematical modeling and simulation of real time transmission of polygon effect on chain drive', *Mechanical Science and Technology for Aerospace Engineering*, Vol. 36, No. 6, pp.821–826.

Zhang, C.W., Peng, X.Q. and Zhang, N. (2012) 'A new method for dynamics analysis on polygon effect of oil saw chain', *Mechanical Science and Technology for Aerospace Engineering*, Vol. 31, No. 3, pp.392–396.

Zhang, H., Kang, P. and Song, Y. (2015) 'Dynamic modeling method and experiment of sliding track walking system', *Vibration, Measurement and Diagnosis*, Vol. 35, No. 1, pp.70–75.

Zhang, X.L., Zhang, H. and Xing, G. (2020) 'Design and simulation of 'Tracked fire fighting robot based on RecurDyn', *Journal of Mechanical Transmission*, Vol. 44, No. 4, pp.89–95.

Zhang, Z.H., Zhang, H. and Chen, Y. (2022) 'Load identification method of crawler travel system based on genetic neural network', *Journal of Vibration and Shock*, Vol. 41, No. 3, pp.54–61+89.